



# Application of green-synthesized cadmium oxide nanofibers and cadmium oxide/graphene nanosheet nanocomposites as alternative and efficient photocatalysts for methylene blue removal from aqueous matrix

Sundararajan Ashok Kumar<sup>1</sup> · Daniel Rani Rosaline<sup>2</sup> · Edson Luiz Foletto<sup>3</sup> · Guilherme Luiz Dotto<sup>3</sup> · Savariroyan Stephen Rajkumar Inbanathan<sup>1</sup> · Gopalan Muralidharan<sup>4</sup>

Received: 10 March 2023 / Accepted: 8 October 2023 / Published online: 23 October 2023  
© The Author(s), under exclusive licence to Springer-Verlag GmbH Germany, part of Springer Nature 2023

## Abstract

For the first time, cadmium oxide (CdO) nanofibers (NFs) and graphene nanosheet (GNS)-doped CdO nanocomposites (NCs) have been synthesized by a simple green route using green tea (*Camellia sinensis*) extract, for subsequent application as photocatalysts for methylene blue (MB) removal from an aqueous matrix. In addition, the materials were tested as working electrodes for supercapacitors. The prepared samples were analyzed by FESEM, UV-Vis spectroscopy, FTIR, and X-ray diffraction (XRD). FESEM revealed that the obtained NPs and NCs show fiber-shaped nanostructure. FTIR confirmed the presence of biomolecules on CdO and carbon compounds on CdO/GNS, while XRD exhibited the cubic crystalline structure of obtained NPs and NCs. The Rietveld refinement using XRD data was performed to ascertain the crystallographic characteristics of the produced samples and look into lattice imperfections. UV-Vis spectroscopy evaluated the optical bandgap energies of CdO and CdO/GNS NCs. The CdO/GNS NCs demonstrated a fast cleavage of the dye molecule under UV irradiation, resulting in 97% removal in 120 min. In addition, CdO/GNS NCs showed remarkable chemical stability as an electrode material, with a high specific capacitance of 231 F g<sup>-1</sup> at a scan rate of 25 mV s<sup>-1</sup>. These observed NCs characteristics are higher when compared to pristine CdO NPs. Finally, we found that the investigated NCs showed enhanced multifunctional properties, such as photocatalytic and supercapacitor characteristics, which can be useful in practical applications.

**Keywords** CdO · CdO/graphene · Green synthesis · Photocatalysis · Methylene blue · Supercapacitor

## Introduction

Toxic and harmful organic compounds in wastewater created by numerous industrial operations cause serious environmental concerns (Georgin et al. 2021a; Jarvin et al. 2021; Jorfi et al. 2016; Khan et al. 2020; Taourati et al. 2020). The full and efficient eradication of hazardous organic pollutants from wastewater has recently received much attention worldwide (Mageshwari et al. 2013). In particular, the hazardous and poisonous dye effluents released by several textile industries significantly threaten our natural ecology (Ajmal et al. 2016; Kumar et al. 2021). Most dye effluents are refractory and non-biodegradable azo dyes, which have carcinogenic properties and can have serious consequences for humans and marine life (Ahmad and Majid 2018; Singh et al. 2019; Tadjarodi et al. 2015). Specifically, methylene blue dye (MB) is widely used in the textile industry, being

---

Responsible Editor: Philippe Garrigues

✉ Guilherme Luiz Dotto  
guilherme\_dotto@yahoo.com.br

- <sup>1</sup> Post Graduate and Research Department of Physics, The American College, Madurai, Tamil Na du 625002, India
- <sup>2</sup> Post Graduate and Research Department of Chemistry, Lady Doak College, Madurai, Tamil Na du 625002, India
- <sup>3</sup> Department of Chemical Engineering, Federal University of Santa Maria, Santa Maria 97105-900, Brazil
- <sup>4</sup> Department of Physics, The Gandhigram Rural Institute (Deemed to be University), Gandhigram, Dindigul, Tamil Na du 624302, India

highly soluble in water and toxic to living beings (Georgin et al. 2021b; Salomón et al. 2021). Conventional wastewater treatment technologies are inefficient and useless due to the dyes' high stability and complicated structure. Dye-containing wastewater is detrimental to the living organisms in the environment and can create problems in the human body, either directly or indirectly (Bhattacharya et al. 2019; Moussavi and Mahmoudi 2009). As a result, removing this contaminant from water is a major problem. In this case, photodegradation of the dye under UV or visible light is an effective route of removing the color from a water body (Jarvin et al. 2023; Mandal et al. 2023; Rane et al. 2019; Santos et al. 2023). In this way, several studies have concentrated on using semiconductor-based photocatalysts to remove organic molecules from wastewater because of their tunable band structure (Brombilla et al. 2022; Chawla et al. 2023; Dutta et al. 2022; Kumar et al. 2023; Sudhaik et al. 2022). However, studies involving the use of cadmium oxide (CdO) nanofibers (NFs) and graphene nanosheet (GNS)-doped CdO nanocomposites (NCs) for methylene blue removal are scarce in the literature.

In recent years, developing efficient energy storage devices has been a practical method to reduce the environmental effect of traditional energy supplies and the rapid rise in global energy demand (Balasingam et al. 2016; Ma et al. 2017; Simon et al. 2020). The rapid advancement of current electronic gadgets and ongoing research into renewable energy-based electrochemical energy conversion systems has fuelled the creation of improved high-performance energy storage technologies (Balasingam et al. 2017). Because of their remarkable properties, such as fast charge/discharge rate, high power density, long cycle life, and improved safety, supercapacitors have been identified as highly promising materials for high-power applications, such as renewable energy systems, digital communications, portable electronics, and hybrid-electric vehicles (Abdah et al. 2020; Jiang et al. 2012; Veerakumar et al. 2020; Zhi et al. 2013). Supercapacitors are divided into two types based on their charge storage mechanisms: electric double-layer capacitors (EDLC), which store energy as accumulating electric charge at the electrode-electrolyte interface, and pseudocapacitor, which stores energy by a fast faradaic redox reaction between electrolyte ions and electrode (Iro et al. 2016; Poudel et al. 2020; Yuan and Zhang 2006). Carbon materials such as graphene and activated carbon are used as electrode materials in EDLC. Conducting polymers and transition metal oxides are employed as electrode materials in pseudocapacitors (Foo et al. 2016). The manufacture of these supercapacitors has mostly relied on transition metal oxides and carbonaceous materials. Transition metal oxides are considered good materials for supercapacitor applications because they have multiple oxidation states for redox charge

transfer (An et al. 2019). Carbon materials benefit from an inherent double layer, whose efficient charging is critical to the supercapacitor's performance. They also have a large surface area, are extremely durable, and have a high mechanical strength (Kim and Kim 2015; Wadekar et al. 2020). Using these two materials to create an asymmetric supercapacitor improves the device's performance synergistically (Ishaq et al. 2019).

Graphene (G) is an allotrope of single-layered carbon atoms arranged in a two-dimensional layer of  $sp^2$ -bonded carbon honeycomb lattice nanostructure (Wei and Liu 2010; Xiang and Yu 2013; Zhou et al. 2021). Although now discovered, G has attracted massive research interest due to its enchanting properties. G shows good electrical and thermal conductivity and has large mechanical strength and high surface area (Kartick and Srivastava 2011; Li et al. 2016). Because of its incredible physical and chemical properties, G has been identified as a hotbed of innovation (An and Jimmy 2011). It can be used in prospective applications, such as electronics, actuators, sensors, and energy storage.

Nowadays, researchers focus on synthesizing nanoparticles (NPs) decorated with graphene nanosheets (GNS) (Albero et al. 2019). Various methods of NP synthesis using different physical and chemical procedures, such as sol-gel, microwave, co-precipitation, and hydrothermal, have been employed (Naseem and Farrukh 2015). These methods require high temperatures and chemical additives. Synthesis of NPs via chemical methods leads to biological risk and is more toxic. Therefore, we need to move on to a safe handling method to avoid these unusual harmful effects. A green method is one of the easiest and most environmentally friendly ways to synthesize NPs using biogenic sources, such as plant, fruit, and leaf extract, and their unrevealed functional biomolecules, which reduce the metal ions into metal NPs (Karthik et al. 2017; Pugazhendhi et al. 2019; Thema et al. 2015). Utilizing the benefits of green synthesis have been used extensively in the synthesis of several nanomaterials. The synthesis of metal oxide NPs is becoming tremendous research in various fields due to their excellent magnetic and thermal properties. Metal oxides, such as MgO, Fe<sub>3</sub>O<sub>4</sub>, ZnO, MnO, TiO<sub>2</sub>, SnO<sub>2</sub>, Ag<sub>2</sub>O, and CoO, are gaining popularity in catalysis, sensors, supercapacitor, and medicinal applications (Balakrishnan et al. 2020; Lazarotto et al. 2020; Nuernberg et al. 2011; Rosaline et al. 2022).

Apart from these metal oxides, cadmium oxide (CdO) is a well-known semiconductor with low resistance and great transmittance on the visible spectrum and is non-toxic (Balamurugan et al. 2016; Shad et al. 2019). CdO is a degenerate n-type semiconductor (Krasil'nikov et al. 2021; Sadhukhan et al. 2019), having both the indirect and direct band gaps of 1.98 eV and 2.5 eV, respectively. Energy storage devices, photocatalyst optoelectronics, phototransistors, photodiodes, solar cells, and gas sensors are some well-known

applications used by CdO NPs (Kaviyarasu et al. 2014; Nasrullah et al. 2020; Shad et al. 2019).

In this present study, the preparation of CdO and CdO/GNS nanocomposites (NCs) by an eco-friendly method using green tea extract has been conducted. Tea extract contains a large number of polyphenolic compounds, which are used in the reduction of metal ions into metal NPs. The predominant organic compound of polyphenol is Epigallocatechin gallate (EGCG), an effective compound that takes part in the reduction process (Gottimukkala et al. 2017; Nagabhushana et al. 2016; Sutradhar et al. 2014). This work represents the potentiality of CdO NFs and CdO/GNS NCs to degrade MB dye, as well as for supercapacitors.

## Experimental procedure

### Synthesis of CdO NPs

CdO NPs were prepared by green route using tea (*Camellia sinensis*) extract. Two grams of the best hand-picked teas from tea bags was dipped in 100 mL of boiling water until the extract was well blended. The extract was then filtered and kept at 5 °C in the beaker for further use. Over a magnetic stirrer, Cd(NO<sub>3</sub>)<sub>2</sub> (0.5 mol L<sup>-1</sup>) was solubilized in 50 mL of distilled water for 2 h. Following the predetermined period, 50 mL of filtered tea extract was slowly added to the Cd(NO<sub>3</sub>)<sub>2</sub> solution. The color was changed to dark brown, and the solution was stirred for 1 h. The mixture was then centrifuged after being rinsed three times with deionized water. After, the mixture was dried for 12 h at 120 °C. The powdered sample was then calcined for 4 h at 400 °C.

### Synthesis of CdO/GNS NCs

The graphene utilized in this study was bought from KNVS incorporation (Nagpur, India). First, 0.25 g of graphene was added to 50 mL of distilled water and magnetically stirred for 1 h at room temperature. Then, the prepared CdO NPs (0.75 g) were incorporated into the mixture and stirred for 3 h. After stirring, the mixture was washed and centrifuged three more times with deionized water. Then, the obtained material was dried at 60 °C for 15 h in a hot air oven. Finally, the material was collected in an air-tight container for further characterization. Figure 1 shows the CdO and CdO/GNS synthesis procedure schematic diagram.

### Characterization techniques

The green-synthesized CdO NPs and CdO/GNS NCs were systematically characterized using several techniques. Fourier-transform infrared (FTIR) analysis was realized on a Jasco 4600 type-A spectrometer at room temperature by

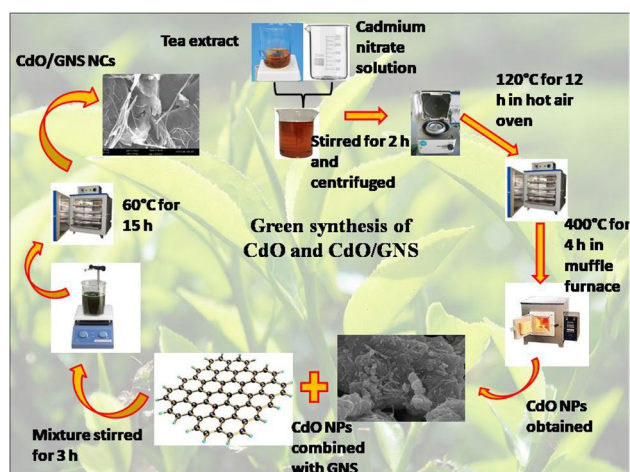


Fig. 1 Schematic diagram of green synthesis of CdO NFs and CdO/GNS NCs

making KBr pellets. X-ray diffraction (XRD) analysis was done on a Rigaku-Ultima III diffractometer, with Cu-K $\alpha$  ( $\lambda = 1.5418 \text{ \AA}$ ) radiation at a grazing angle 1° and stepped size of 0.01°. FESEM images were obtained on a Hitachi-Japan S-3000H scanning electron microscope. The optical properties of the materials were recorded from UV-Vis spectrometer spectrophotometer LI-295, 8 W, 50 Hz.

### Photocatalytic tests

The photocatalytic activities of CdO and CdO/GNS were investigated on the MB degradation under UV light using an artificial UV lamp (11 W). First, an initial concentration of MB solution of 10 mg/L was prepared. Then, 25 mg of CdO and CdO/GNS was added to each 100 mL dye solution. Before UV irradiation, the suspension (dye + photocatalyst) was stirred for 30 min in the dark to reach an equilibrium between the MB and photocatalyst. After dark stirring, the reaction mixture was exposed to UV light. About 5 mL of suspension was taken at each 20 min and centrifuged to separate the phases. The dye degradation efficiency was calculated using the UV-Vis spectrophotometer (Jasco, LI-295) at 664 nm. The degradation efficiency was obtained by Eq. 1 (Jarvin et al. 2021; Pugazhendhi et al. 2019):

$$\text{Degradation, \%} = \frac{C_o - C_t}{C_o} \times 100 \quad (1)$$

$C_o$  is the initial MB concentration, and  $C_t$  is the MB concentration after degradation.

The photocatalytic assays were performed in triplicate. The experimental error was below 5.5%.



## Electrochemical studies

The electrochemical behaviors of CdO NFs and CdO/GNS NCs were observed on an electrochemical workstation with a three-electrode cell set-up (CHI660D, Champaign, IL) at room temperature. The electrochemical performance of the as-prepared electrodes has been examined by electrochemical impedance spectroscopy (EIS), cyclic voltammetry (CV), and galvanostatic charge-discharge (GCD). The modified nickel foam (NF) substrate with the active material CdO NFs and CdO/GNS NCs was used as a working electrode, Ag/AgCl electrode as a reference electrode, and platinum wire as a counter, respectively. A modified working electrode was fabricated by mixing synthesized samples, acetylene black (conductive induction), and binder polytetrafluoroethylene (PTFE) in mass ratios (85:10:05). The substances were ground by using agate mortar and pestle. Ethanol solvent was also used to make the paste. The mass of the active material is used as 2 mg. The collected paste was coated on the surface of the nickel foam (1×1 cm<sup>2</sup>) and allowed to dry at 80 °C for 12 h. 6M of KOH solution was employed as an aqueous electrolyte for the electrochemical experiment. The potential window ( $\Delta V$ ) was applied from -0.7 to 0.3 V for the experiment. The specific capacitance ( $C_{sp}$ ) was obtained from CV (Eq. 2) and GCD (Eq. 3) curves, using Eqs. 2 and 3 (Balasingam et al. 2016; Balasingam et al. 2017):

$$C_{sp} = \frac{\int I(V)dv}{sm\Delta V} (\text{F g}^{-1}) \quad (2)$$

$$C_{sp} = \frac{I\Delta t}{m\Delta V} (\text{F g}^{-1}) \quad (3)$$

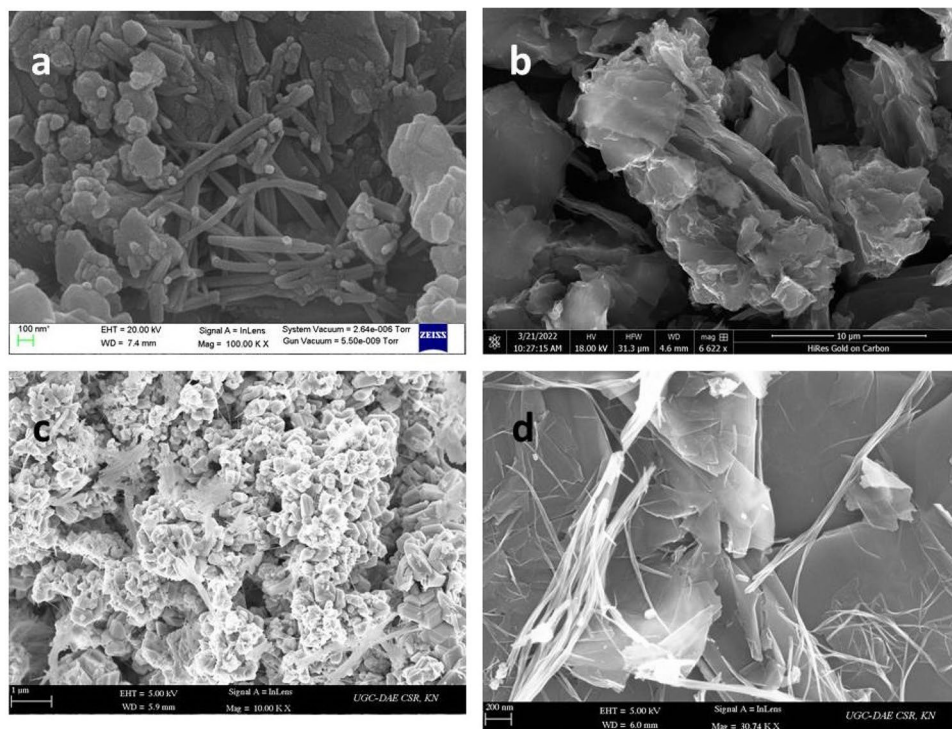
where  $C_{sp}$  is the specific capacitance (F g<sup>-1</sup>),  $I$  is the discharge current (A),  $m$  is the mass of the material (g),  $s$  is the scan rate (mV s<sup>-1</sup>),  $\int I(V)dv$  is the integrated area of the CV curve,  $\Delta V$  is the potential window (V), and  $\Delta t$  is discharge time (s).

## Results and discussion

### FESEM

The morphology of CdO, Gr, and G-CdO nanomaterials was obtained by FESEM, as shown in Fig. 2a–d. From FESEM analysis, the green-synthesized pure CdO nanopowder at the temperature of 400 °C for 4 h shows a nanofiber (NFs) like structure (Fig. 2a). As shown in Fig. 2b, the FESEM image of Gr suggests a lamellar nanosheet (GNS) like the structure of Gr with the monolayer. After adding GNS with CdO NFs, the temperature of 60 °C for 15 h resulted in CdO NFs being well decorated on the surface of GNS. Figure 2c and d show the different magnifications of CdO/GNS NCs. The average diameter and length of the pure CdO NFs were found to be 43.7 ± 2 nm and 399 ± 6 nm, respectively. The FESEM results obtained from CdO/GNS NCs diameter and length were 25 ± 7 nm and 756 ± 4 nm, respectively. The particle size of CdO/GNS NCs is lesser than pure CdO NFs, which

**Fig. 2** FESEM results of **a** CdO NFs, **b** graphene nanosheets, and **c, d** CdO/GNS NCs at different magnifications



results in NCs with a larger specific surface area. Hence, the as-prepared NCs can be used as photocatalysts and electrodes for supercapacitor applications.

## FTIR

FTIR technique is useful for identifying different functional groups on graphene and its composites. Figure 3 represents the typical FTIR spectrum of synthesized CdO NFs and CdO/GNS NCs. The bands at 3594, 3521, and 3438  $\text{cm}^{-1}$  are assigned to the O-H group of water molecules (Balaramurugan et al. 2016; Krasil'nikov et al. 2021; Shad et al. 2019) present on the CdO and CdO/GNS NCs. The band at 3230  $\text{cm}^{-1}$  indicated the presence of the N-H stretching vibrational group. Also, the band at 1423  $\text{cm}^{-1}$  is assigned to the presence of O-H bonding of water molecules. The metal-oxide stretching vibration of CdO was observed at 957, 864, and 697  $\text{cm}^{-1}$  (Kaviyarasu et al. 2014; Nasrullah et al. 2020). From the G-CdO FTIR spectrum, the absorption band at 1633 corresponds to the C=C stretching of graphene (Hassanien et al. 2019; Husein et al. 2021). As a result, CdO and G-CdO exhibit the same absorption peak range, and no band shifts were observed after adding graphene.

## XRD

Figure 4 shows the XRD patterns of CdO NPs and CdO/GNS NC samples. CdO NPs exhibit various diffraction peaks at  $2\theta = 32.99^\circ, 38.28^\circ, 55.25^\circ, 65.87^\circ,$  and  $69.2^\circ$ , corresponding to the crystal planes (111), (200), (220), (311), and (222) of CdO, respectively. The diffraction peaks could be matched with the CdO single-phase cubic structure (Karthik et al.

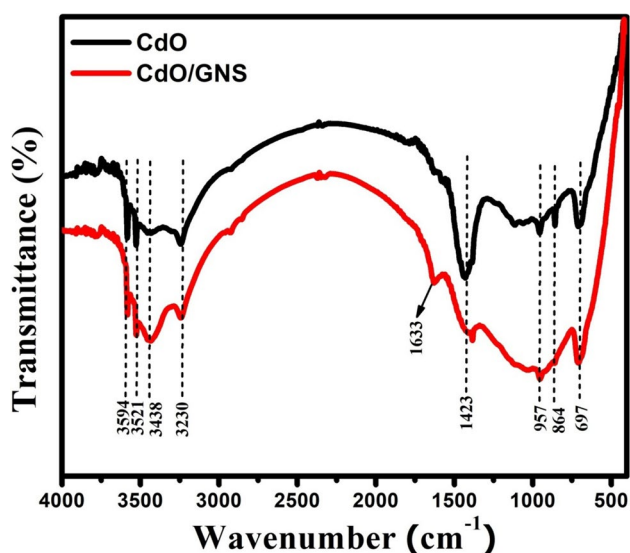


Fig. 3 FTIR spectra of CdO NFs and CdO/GNS NCs

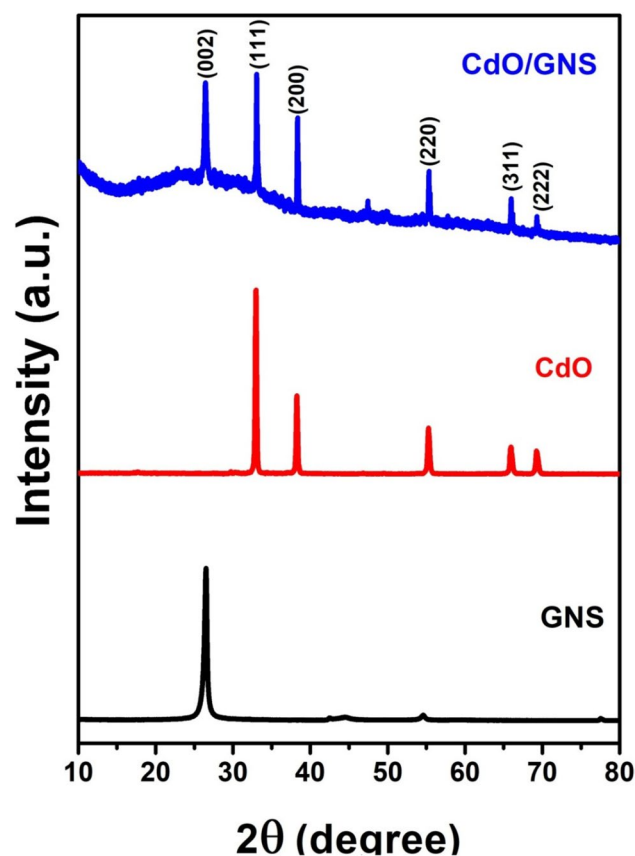


Fig. 4 XRD patterns of graphene, CdO NFs, and CdO/GNS NCs

2017; Nasrullah et al. 2020) by comparison with the JCPDS card file 01-073-2245. The diffraction planes of CdO were indexed with lattice constant  $a = 4.6990 \text{ \AA}$  and belonged to the space group of Fm-3m (225), indicating the pure crystalline of CdO NPs. A prominent peak confirmed the exfoliation of graphite into graphene layers at  $2\theta = 26.45^\circ$ , linked to the (002) plane with d-spacing 3.368  $\text{Å}$  in graphene XRD investigation (Hassanien et al. 2019; Husein et al. 2021). The anchoring of CdO nanoparticles onto GNS is reflected in the diffractogram of CdO/GNS, which is identical to graphene and hybrid CdO NPs. The average crystallite sizes of CdO NFs and CdO/GNS NCs were  $48 \pm 3$  and  $41.62 \pm 6$  nm, respectively.

## Rietveld refinement

Figure 5a and b show the Rietveld refinement of CdO NFs and CdO/GNS NCs using XRD data. Rietveld analysis has been carried out using the Pseudo-Voigt shape function by FULLPROOF software. Pseudo-Voigt approximation of the Voigt function is perhaps the most extensively utilized for examining the X-rays of the analytical peak functions. The pseudo-Voigt function is an amalgam of Gaussian and

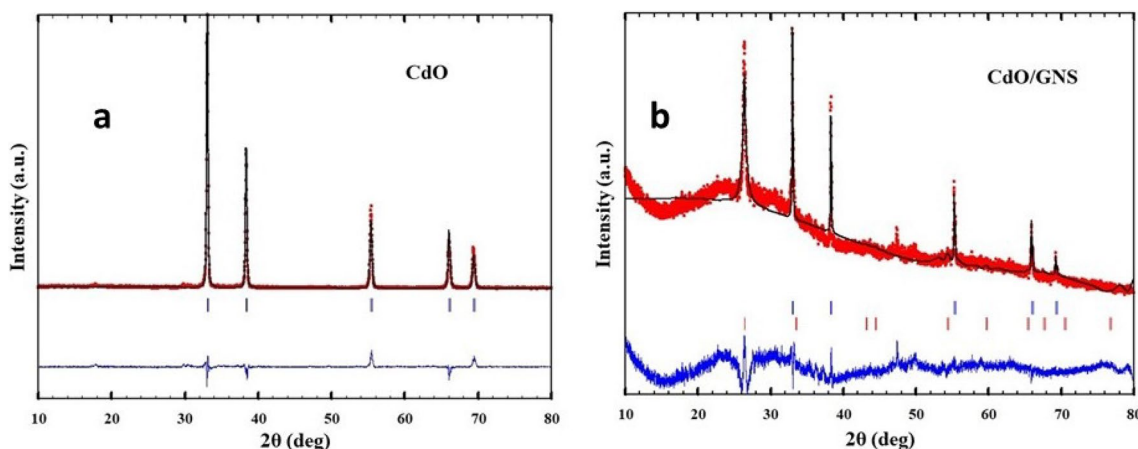


Fig. 5 Rietveld refinement of (a) CdO NFs and (b) CdO/GNS NCs

Table 1 Reliability factors of CdO NFs and CdO/GNS NCs

| Parameters                | CdO    | CdO/GNS   |
|---------------------------|--------|-----------|
| $R_p$                     | 20.7   | 51.9      |
| $R_{wp}$                  | 23.1   | 34.8      |
| $R_{exp}$                 | 14.78  | 16.9      |
| $GoF$                     | 1.56   | 2.059     |
| $\chi^2$                  | 2.43   | 4.242     |
| $a$                       | 4.6895 | 2.33219   |
| $b$                       | 4.6895 | 5.34087   |
| $c$                       | 4.6895 | 6.749072  |
| $\alpha = \beta = \gamma$ | 90     | 90        |
| Phase: 1                  | Cubic  | Cubic     |
| Volume of the cell        | 103.18 | 103.565   |
| Phase: 2                  | -      | Hexagonal |
| Volume of the cell        | -      | 84.066    |

Lorentzian elements in the ratio of  $\eta/(1-\eta)$ , where  $\eta$  is the Pseudo-Voigt mixing parameter. From Fig. 5b, the observed (black), calculated (red), and difference (blue bottom) profiles show that the characteristic difference profile for intensity is either positive or negative and concentrated at the center of the peak. Although the difference profile plot is likely the best method to follow and guide a Rietveld refinement, the numerical fit of the computed pattern to the actual data can also be presented. This result is commonly expressed in terms of  $R$  values. The obtained  $R$  values, such as pattern reliability factor ( $R_p$ ), weighted profile  $R$ -value ( $R_{wp}$ ), expected  $R$ -value ( $R_{exp}$ ), chi-squared value ( $\chi^2$ ), and goodness of fit ( $GoF$ ), are given in Table 1.  $GoF$  can be calculated from the ratio of  $R_{wp}$  and  $R_{exp}$  (i.e.)  $GoF = R_{wp} / R_{exp}$ .  $\chi^2$ , which is defined by  $(GoF)^2 = \chi^2$  (Mariammal et al. 2011; McCusker et al. 1999).

### UV-Vis analysis

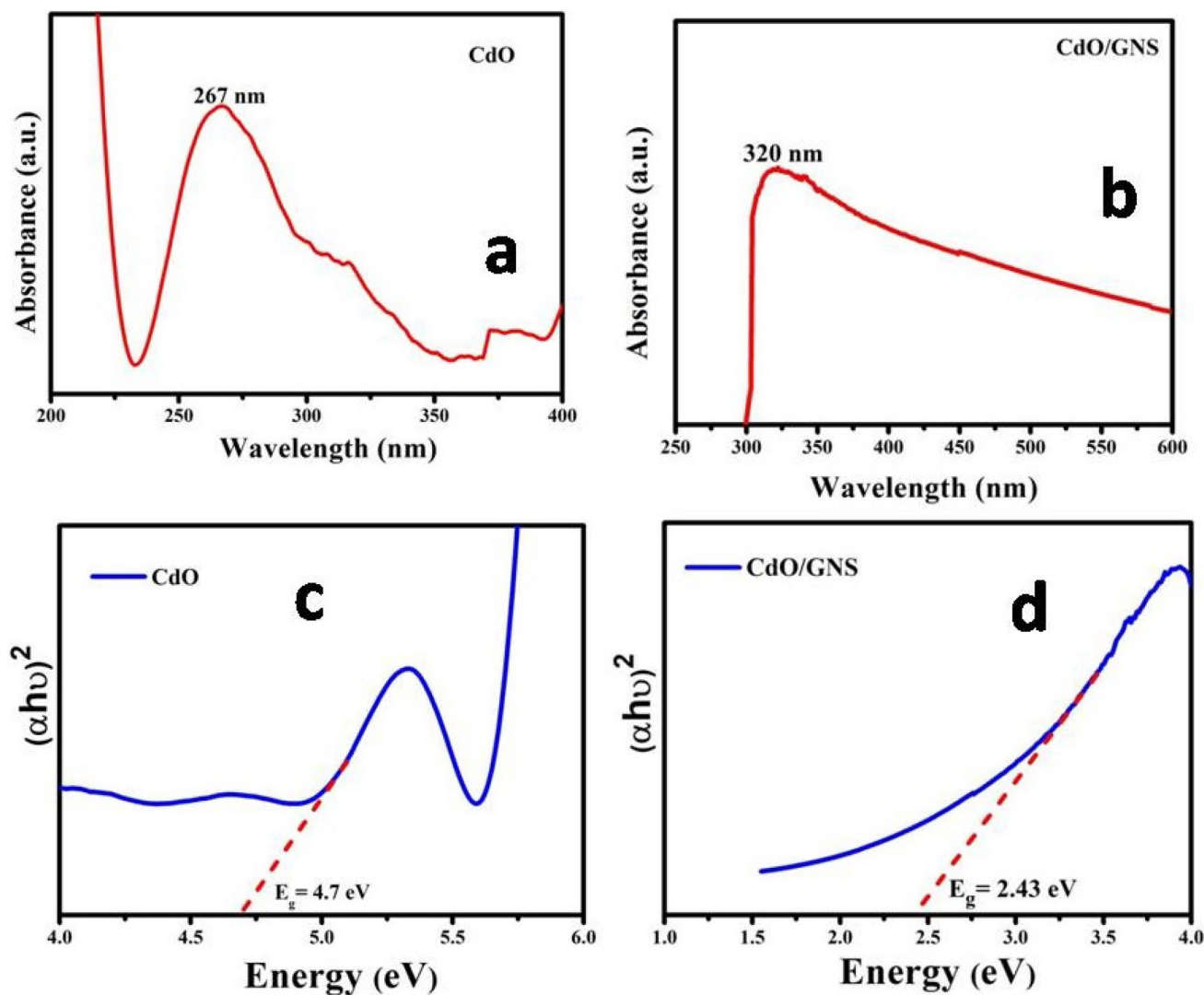
Figure 6 depicts the optical absorption spectra of CdO NFs and CdO/GNS NCs. The samples were previously ultrasonicated in distilled water for posterior analysis. CdO exhibits the absorption peak located at 267 nm (Fig. 6a), which is attributed to the interband transition of a deep level of valence band electrons and assigned to the excitonic feature of CdO (Kumar et al. 2016). After adding GNS to CdO, the absorption peak shifted to 320 nm (Fig. 6b), reflecting the quantum confinement effect of the NCs (Hassanien et al. 2019; Husein et al. 2021). The energy bandgap was calculated by Eq. 4 (Hassanien et al. 2019):

$$\alpha h\nu = A(h\nu - E_g) \tag{4}$$

where  $\alpha$  is the absorption coefficient,  $\nu$  is the frequency of light,  $h$  is Planck’s constant,  $A$  is the constant,  $E_g$  is the energy bandgap, and  $n$  is the transition process involved ( $n = 2$  for direct electron transition, and  $n = 1/2$  for indirect electron transition). The bandgap energies for pristine CdO NFs and CdO/GNS NCs are 4.7 and 2.43 eV, respectively (Fig. 6c, d). The greater absorption and lower energy bandgap of CdO/GNS NCs raise the possibility that, when exposed to UV light, they may have a better photocatalytic degradation efficiency for the target pollutants (Silvestri et al. 2019a; Umar et al. 2022).

### Photocatalytic studies

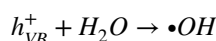
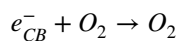
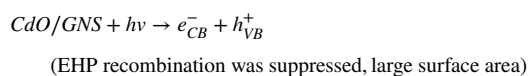
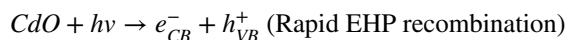
The catalytic efficiencies of CdO and CdO/GNS NCs towards MB dye photodegradation are shown in Fig. 7a and b, respectively. Under the stimulated UV irradiation, the valence band (VB) electrons ( $e^-$ ) of CdO are excited to the conduction band



**Fig. 6** UV-Vis spectra of (a) CdO NFs and (b) CdO/GNS NCs, and bandgap energies of (c) CdO NFs and (d) CdO/GNS NCs

(CB), leaving holes ( $h^+$ ) in the VB, creating the formation of  $e^-/h^+$  pairs (EHPs). The photogenerated  $e^-$  and  $h^+$  subsequently undergo redox processes, resulting in many active species. The photogenerated  $e^-$  reacts with dissolved molecular oxygen, generating superoxide ions ( $O_2^-$ ). The formation of  $h^+$  also reacts with water ( $H_2O$ ) and hydroxide ions ( $OH^-$ ) to form highly reactive hydroxyl radicals ( $\bullet OH$ ). The  $O_2^-$  and  $\bullet OH$  radicals have high oxidation performance, completely oxidizing the dye molecules, resulting in final products like  $CO_2$  and  $H_2O$  (Ahmad and Majid 2018; Kumar et al. 2016; Singh et al. 2019). The degradation efficiency of pure CdO NFs towards MB dye was 94% in 160 min under UV irradiation. On the other hand, CdO/GNS NCs have a maximum degradation efficiency of 97% in 120 min (Fig. 7c). This may be assigned to a larger active surface area of CdO/GNS NCs when compared to CdO NFs after CdO was decorated on the GNS, which is an excellent  $e^-$  acceptor and conductor. Under UV

irradiation, the  $e^-$  are generated by the photons and are readily transferred from CdO CB to GNS, which could suppress the recombination rate of EHPs (Umar et al. 2022). Therefore, the photocatalytic performance of CdO/GNS was greater than pure CdO NFs. The proposed mechanism of the photocatalytic process is given below.





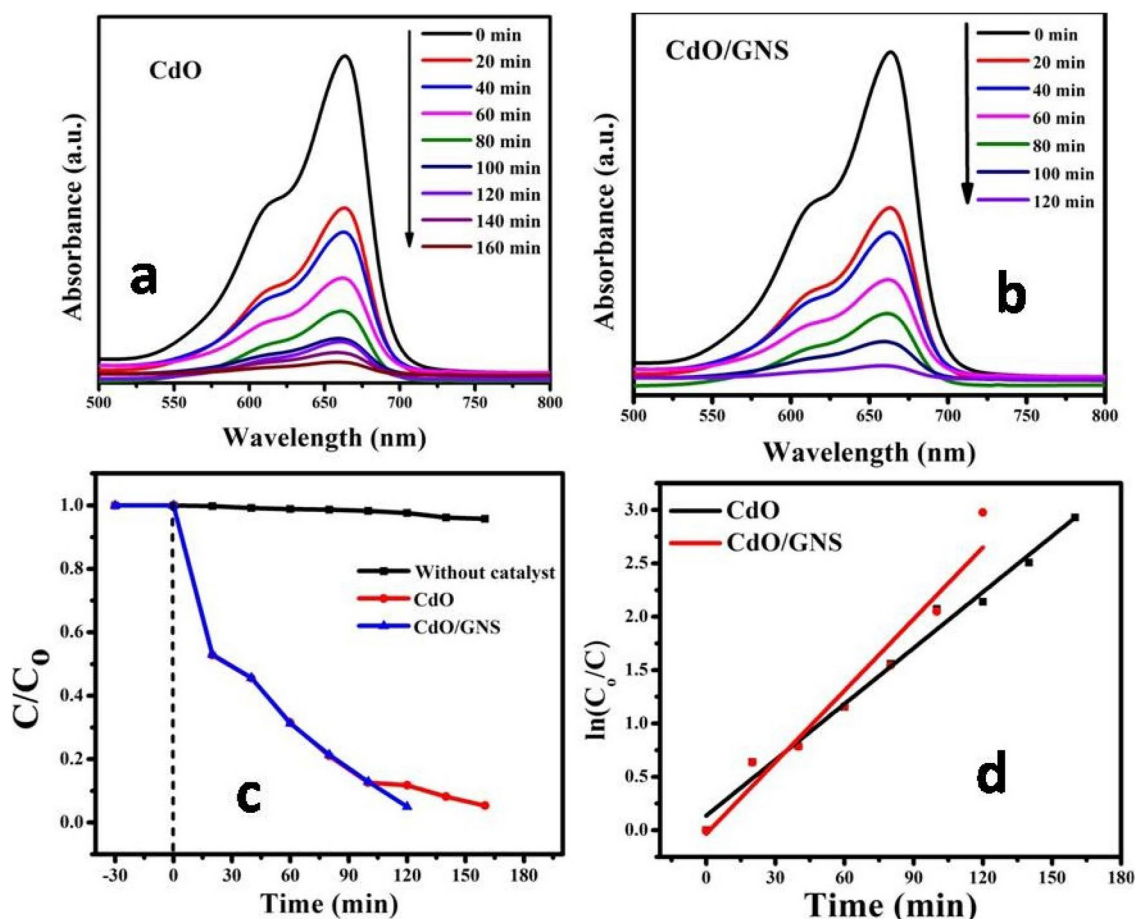


**Fig. 7** Photocatalytic activity of (a) CdO NFs and (b) CdO/GNS NCs, c degradation efficiency graph, and (d) kinetic graphs of CdO and CdO/GNS NCs

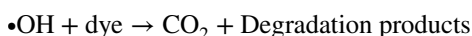


Figure 7d shows the kinetic graph of CdO NFs and CdO/GNS NCs. Kinetic models can determine the degradation rate constant of organic molecules on semiconducting materials. It was observed that both CdO NFs and CdO/GNS NCs presented a degradation process following pseudo-first-order (PFO) kinetics (Jarvin et al. 2021; Vieira et al. 2022). The PFO kinetics is given by Eq. 5:

$$\ln \frac{C_o}{C} = k_{app}t \tag{5}$$

where  $k_{app}$  is the apparent rate constant for PFO kinetics,  $C_o$  is the initial dye concentration after dark adsorption, and  $C$  is the dye concentration after a certain reaction time  $t$ .

The determination coefficient ( $R^2$ ) and the  $k_{app}$  were evaluated and compared in Table 2. As a result, it is possible to observe that the  $k_{app}$  for CdO/GNS NCs was 1.28 times higher than the  $k_{app}$  of CdO NFs. According to the previous results, an illustrative diagram of the photocatalytic mechanism toward MB degradation was proposed and is shown in Fig. 8.

In order to demonstrate the remarkable photocatalytic activity of CdO/GNS NCs towards MB degradation, the photocatalytic efficiency of CdO/GNS NCs was compared with some recently reported photocatalysts, as represented in Table 3. According to the results presented in Table 3, it is possible to infer that the material produced in this work

**Table 2** Reaction rate constants and correlation coefficients for CdO and CdO/GNS NCs

| Material | $k_{app}$ (min <sup>-1</sup> ) | $R^2$  |
|----------|--------------------------------|--------|
| CdO      | 0.0175                         | 0.9851 |
| CdO/GNS  | 0.0224                         | 0.9682 |



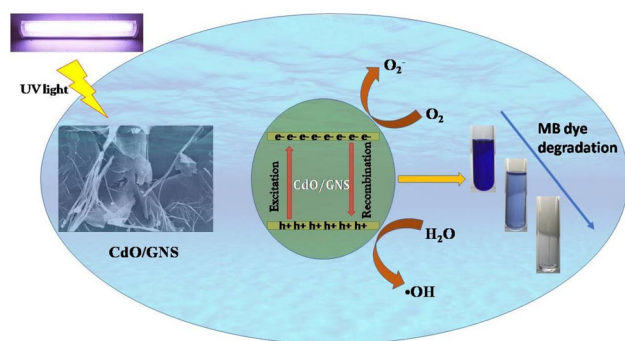


**Fig. 8** Photocatalytic degradation mechanism of MB dye

exhibits great potential for application as a photocatalyst for the abatement of pollutant organic molecules from wastewater.

### Electrochemical studies

The electrochemical performances of CdO NFs and CdO/GNS NCs electrodes were determined by CV, GCD, and EIS spectroscopy techniques using 6 M of KOH electrolyte solution (Fig. 9). The CV characterization for CdO NFs and CdO/GNS NCs under different scan rates (25 to 150 mV/s) is shown in Fig. 9a, b. All the CV curves are within the range of  $-0.7$  to  $0.3V$ . The CV curve of pristine CdO shows a non-rectangular shape, which is attributed to the redox reaction occurring on the active electrode surface (Fig. 9a). A pair of redox peaks appeared, and it clearly states that the electrode is pseudo-capacitance (Balasingam et al. 2016; Balasingam et al. 2017). From Fig. 9a, it is seen that the scan rate is increasing from lower to higher, and

simultaneously, current densities of oxidation and reduction peaks are increased and shifted. It is due to the reversible reaction at the surface of the active electrode. The redox peaks are noticeable at a high scan rate of 150 mV/s, with no obvious distortion. From Fig. 9b, the shape of CV curves for the CdO/GNS NCs sample divulged the quasi-rectangular behavior, which involved faradaic redox reactions (Kumar et al. 2017; Packiaraj et al. 2019). The graph distinguishes pseudo-capacitance nature with the high surface area due to the presence of GNS material. Hence, the charge storage mechanism was used to analyze the appearance of faradaic redox reactions on the surface of the active electrode. The specific capacitance of CdO and CdO/GNS were calculated from the CV curves using Eq. (2). The specific capacitance values for CdO at scan rates of 25, 50, 75, 100, 150 mV/s are found to be 203, 178, 160, 139, and 116  $F g^{-1}$ , and for CdO/GNS NCs, they are found to be 231, 207, 180, 165, and 140  $F g^{-1}$ , respectively. The specific capacitance value of CdO/GNS NCs is much higher than CdO NFs. Due to the following features (Balasingam et al. 2016): (i) the CdO/GNS NCs provide more electroactive sites for store charges through EDLC, as well as faradaic reaction (ii) fast charge transfer is made possible by the CdO anchored on the GNS, which effectively minimized the agglomeration of the electroactive components and decreased internal resistance. The obtained specific capacitance value calculated from CV is higher than earlier reported by Kumar et al. (2017).

Figure 9c and d show the GCD profiles of CdO NFs and CdO/GNS NCs under different current densities with 6 M KOH electrolytes. Generally, linear and non-linear discharge areas can categorize discharge behavior. While charge storage occurs in the first type based on an adsorption/desorption process, the second type occurs due to a

**Table 3** Comparison of degradation efficiencies of MB dye for different photocatalysts

| Photocatalyst                          | Dye concentration (mg L <sup>-1</sup> ) | Catalyst dosage (g L <sup>-1</sup> ) | Irradiation source | Time (min) | Degradation efficiency (%) | Reference                |
|--|---|--------------------------------------|--------------------|------------|----------------------------|--------------------------|
| Mn <sub>3</sub> O <sub>4</sub> /rGO    | 1                                       | 0.02                                 | Sunlight           | 120        | 60                         | Jarvin et al. (2021)     |
| MgO                                    | 15                                      | 0.05                                 | UV light           | 240        | 99                         | Mageswari et al. (2013)  |
| CdO/GO                                 | 25                                      | 0.025                                | Visible            | 90         | 91                         | Ahmad and Majid (2018)   |
| Ag-doped ZnO                           | 1                                       | 0.079                                | Sunlight           | 30         | 95                         | Jarvin et al. (2022)     |
| TiO <sub>2</sub> /biochar              | 10                                      | 1                                    | UV light           | 180        | 80                         | Silvestri et al. (2020)  |
| Zn <sub>2</sub> SnO <sub>4</sub>       | 10                                      | 1                                    | UV light           | 25         | 96                         | Silvestri et al. (2019b) |
| CdO/rGO                                | 0.4                                     | 0.05                                 | UV light           | 110        | 80                         | Kumar et al. (2016)      |
| Fe <sub>3</sub> O <sub>4</sub> /GO     | 1                                       | 0.03                                 | Sunlight           | 30         | 91                         | Umar et al. (2022a)      |
| Poly(1-naphthylamine)                  | 5                                       | 0.1                                  | UV light           | 160        | 61                         | Umar et al. (2022b)      |
| CdO/Cds                                | 0.4                                     | 0.05                                 | UV light           | 100        | 71                         | Kumar et al. (2017)      |
| Cr-Co-doped CdO                        | 5                                       | 0.02                                 | Sunlight           | 60         | 99.5                       | Munawar et al. (2021)    |
| Cu-Cu <sub>2</sub> O-Cu <sub>3</sub> N | 5                                       | 0.25                                 | Sunlight           | 360        | 96                         | Paredes et al. (2023)    |
| Fe/CdO                                 | 10                                      | 0.01                                 | UV light           | 130        | 87                         | Mandal et al. (2023)     |
| CdO/GNS                                | 10                                      | 0.025                                | UV light           | 120        | 97                         | Present work             |

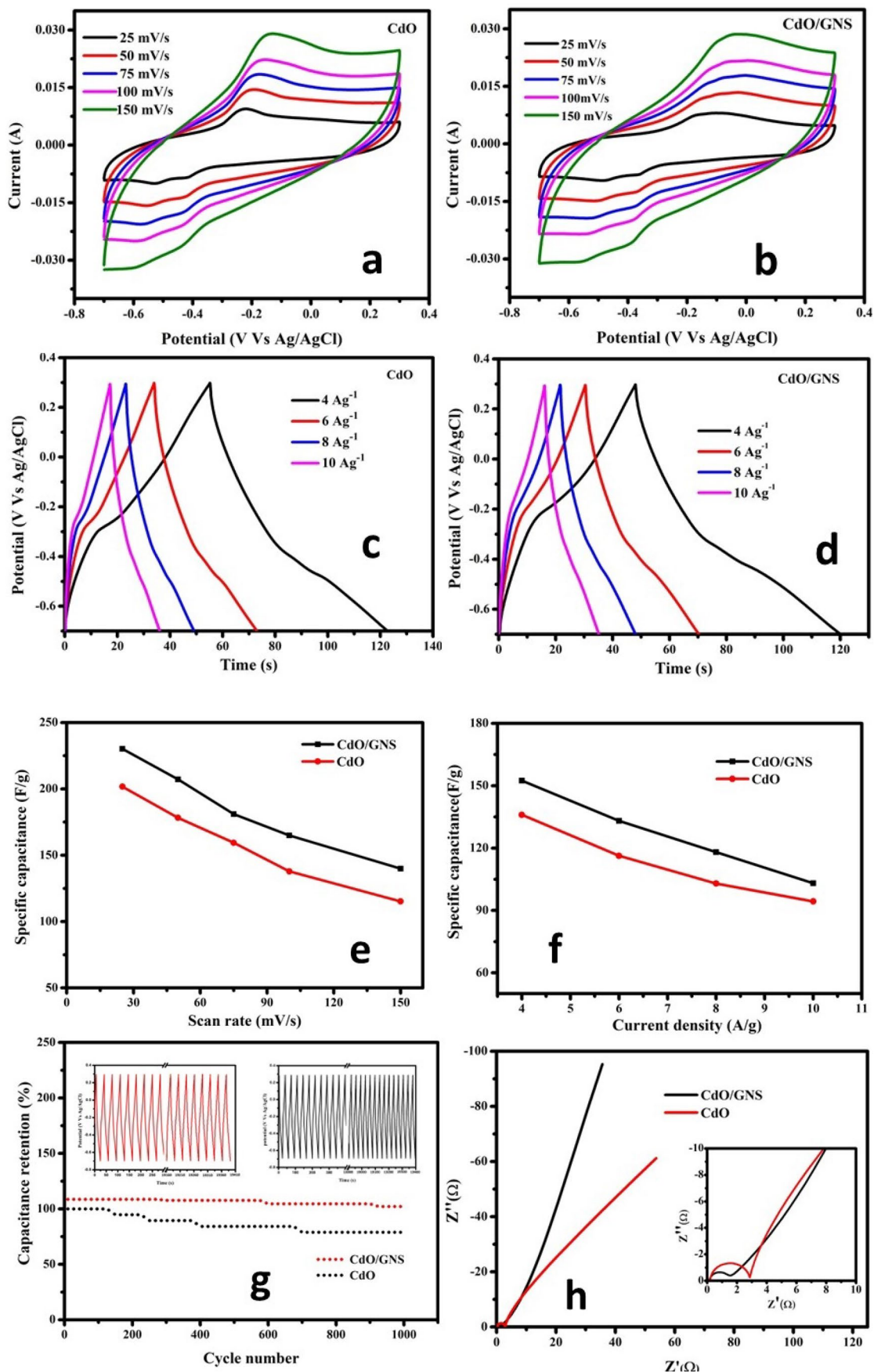


**Fig. 9** CV graphs of (a) CdO NFs and (b) CdO/GNS NCs at different scan rates, GCD graphs of (c) CdO NFs and (d) CdO/GNS NCs at different current densities, e specific capacitance vs. scan rate and (f) specific capacitance vs. current densities for CdO NFs and CdO/GNS NCs, and (g) cycle stability and (h) EIS graph for CdO NFs and CdO/GNS NCs

pseudocapacitive mechanism. Figure 9c represents the GCD profile for pure CdO, which shows the pseudocapacitive nature. Figure 9d represents the GCD graph of CdO/GNS NCs, clearly showing a nearly triangular shape with a voltage plateau, demonstrating both the EDLC and the pseudocapacitance contributions (Balasingam et al. 2016; Balasingam et al. 2017). The GCD plot of NCs electrode shows more discharge time than pure CdO, resulting in the active electrode's large storage capacity. The specific capacitance values for CdO NFs and CdO/GNS NCs were calculated by Eq. (3). The specific capacitance values of CdO NFs at various current densities of 4, 6, 8, and 10 A g<sup>-1</sup> were 136, 116, 103, and 95 F g<sup>-1</sup>, respectively. The values for CdO/GNS NCs are 153, 133, 118, and 103 F g<sup>-1</sup> for the same current densities. The capacitance values of NCs are higher than NFs due to the high surface area of GNS. The charge-discharge profile displayed a linear discharge, indicating that the hybrid active material presents electrochemical behavior via EDLC and pseudo-capacitance reactions. In contrast to increasing discharge current densities, the predicted specific capacitance values are decreasing. This trend is because, at greater current densities, the faradaic redox reaction between the electrolyte and electrode surface does not have enough time to complete, which leads to an increase in resistance (Umar et al. 2022; Packiaraj et al. 2019; Kumar et al. 2017). Figure 9e and f represent the calculated capacitance values of CdO NFs and CdO/GNS NCs, corresponding to different scan rates and current densities. The obtained specific capacitance value calculated from GCD is higher than earlier reported by Munawar et al. (2021).

The cyclic performance of the modified electrode was carried out by charge-discharge at a current density of 0.01 Ag<sup>-1</sup> for 1000 cycles. Figure 9g reveals the cyclic stability of CdO NFs and CdO/GNS NC electrodes. After 1000 cycles, only 70% was retained by the CdO NFs, but CdO/GNS NC electrodes obtained 90% retention after 2000 cycles. The electrochemical reaction process is further studied by EIS analysis, mainly used to investigate the ion movement between electrolyte and electrode surface with an amplitude of 5 mV in a frequency range from 0.01 Hz to 100 kHz. Figure 9h shows the Nyquist plots of the CdO NFs and CdO/GNS NC electrodes after 1000 cycles GCD. In the high-frequency region, CdO displays a small semicircle with the spike on the Z'-real axis representing the equivalent series resistance (ESR). The spike is associated with the electrolyte solution's diffusion resistance on the electrode surface. The

diameter of the semicircle represents the interfacial charge transfer resistance ( $R_{ct}$ ) (Balasingam et al. 2016; Balasingam et al. 2017; Umar et al. 2022). CdO/GNS NCs show a very small semicircle with a spike at the low-frequency region. The inclined line at the low-frequency region indicates the diffuse resistance of electrolyte ions inside the electrode materials. The ESR values of the pristine CdO and CdO/GNS NCs before and after the cycling test were determined to be 0.205  $\Omega$  and 0.161  $\Omega$ . The  $R_{ct}$  values for CdO and CdO/GNS materials were 2.7  $\Omega$  and 1.5  $\Omega$ , respectively. Compared to CdO, CdO/GNS NCs electrode presented lower ESR and  $R_{ct}$  values, designating the good ionic conductivity and excellent charge transport of electrolyte ions (Munawar et al. 2021).

## Conclusions

CdO NFs and CdO/GNS NCs were successfully prepared by a simple green method using tea extract as a reducing agent. The length and the diameter of the CdO NFs and CdO/GNS NCs were calculated using FESEM images. CdO NFs are well decorated in the GNS. FTIR spectrum confirms the presence of C=C stretching of graphene, and CdO peaks are observed in the CdO/GNS NCs with no shift. XRD pattern exhibits the cubic crystalline structure of CdO NFs and the presence of GNS. Rietveld refinement provides the reliability factors of CdO and CdO/GNS NCs. UV-Vis spectrum shows that the energy bandgap of CdO/GNS NCs was comparatively lower than pristine CdO NFs, resulting in better photocatalytic efficiency for CdO/GNS NCs. In addition, the larger surface area for CdO/GNS NCs contributed to its better photocatalytic performance towards MB dye degradation under UV irradiation. The high specific capacitance achieved by green-synthesized CdO/GNS was 231 F g<sup>-1</sup> at 25 mV s<sup>-1</sup>. After the 1000 cycles, the active electrode CdO/GNS NCs exhibit 90% chemical stability. Compared to pure CdO NPs, the observed features of the NCs are higher. In the end, we found that the examined NCs exhibited improved multifunctional qualities, including photocatalytic and supercapacitor features, which can be highly helpful in real-world applications.

**Author contribution** Conceptualization: Sundararajan Ashok Kumar; methodology: Savariroyan Stephen Rajkumar Inbanathan, Daniel Rani Rosaline, Formal analysis and investigation: Savariroyan Stephen Rajkumar Inbanathan, Gopalan Muralidharan, Daniel Rani Rosaline; writing—original draft preparation: Sundararajan Ashok Kumar, Savariroyan Stephen Rajkumar Inbanathan; writing—review and editing: Guilherme Luiz Dotto, Edson Luiz Foletto; funding acquisition: Savariroyan Stephen Rajkumar Inbanathan; supervision: Savariroyan Stephen Rajkumar Inbanathan. All authors read and approved the final manuscript.



**Funding** This work was supported by the UGC-DAE Consortium for Scientific Research Indore Center grant Ref: CSR IC -236/2017-18/1317 (Dated 31 March 2018). The Brazilian authors received financial support from CAPES (Coordination for the Improvement of Higher Education Personnel) and CNPq (National Council for Scientific and Technological Development).

**Data availability** The datasets used and analyzed during the current study are available from the corresponding author on reasonable request.

## Declarations

**Ethical approval** Not applicable.

**Consent to participate** Not applicable.

**Consent for publication** Not applicable.

**Competing interests** Guilherme Luiz Dotto declares that he is Associate Editor of Environmental Science and Pollution Research. The other authors declare that they have no competing interests.

## References

- Abdah MAAM, Azman NHN, Kulandaivalu S, Sulaiman Y (2020) Review of the use of transition-metal-oxide and conducting polymer-based fibres for high-performance supercapacitors. *Mater Des* 186:108199. <https://doi.org/10.1016/j.matdes.2019.108199>
- Ahmad J, Majid K (2018) Enhanced visible light driven photocatalytic activity of CdO-graphene oxide heterostructures for the degradation of organic pollutants. *New J Chem* 42(5):3246–3259. <https://doi.org/10.1039/C7NJ03617E>
- Ajmal A, Majeed I, Malik RN, Iqbal M, Nadeem MA, Hussain I, Nadeem MA (2016) Photocatalytic degradation of textile dyes on Cu<sub>2</sub>O-CuO/TiO<sub>2</sub> anatase powders. *J Environ Chem Eng* 4(2):2138–2146. <https://doi.org/10.1016/j.jece.2016.03.041>
- Albero J, Mateo D, García H (2019) Graphene-based materials as efficient photocatalysts for water splitting. *Molecules* 24(5):906. <https://doi.org/10.3390/molecules24050906>
- An C, Zhang Y, Guo H, Wang Y (2019) Metal oxide-based supercapacitors: progress and perspectives. *Nanoscale Adv* 1(12):4644–4658. <https://doi.org/10.1039/C9NA00543A>
- An X, Jimmy CY (2011) Graphene-based photocatalytic composites. *RSC Advances* 1(8):1426–1434. <https://doi.org/10.1039/C1RA00382H>
- Balakrishnan G, Velavan R, Batoo KM, Raslan EH (2020) Microstructure, optical and photocatalytic properties of MgO nanoparticles. *Results Phys* 16:103013. <https://doi.org/10.1016/j.rinp.2020.103013>
- Balamurugan S, Balu AR, Usharani K, Suganya M, Anitha S, Prabha D, Ilangoan S (2016) Synthesis of CdO nanopowders by a simple soft chemical method and evaluation of their antimicrobial activities. *Pacific Science Review A: Nat Sci Eng* 18(3):228–232. <https://doi.org/10.1016/j.psr.a.2016.10.003>
- Balasingam SK, Lee JS, Jun Y (2016) Molybdenum diselenide/reduced graphene oxide based hybrid nanosheets for supercapacitor applications. *Dalton Trans* 45(23):9646–9653. <https://doi.org/10.1039/C6DT00449K>
- Balasingam SK, Lee M, Kim BH, Lee JS, Jun Y (2017) Freeze-dried MoS<sub>2</sub> sponge electrodes for enhanced electrochemical energy storage. *Dalton Trans* 46(7):2122–2128. <https://doi.org/10.1039/C6DT04466B>
- Bhattacharya D, Ghoshal D, Mondal D, Paul BK, Bose N, Das S, Basu M (2019) Visible light driven degradation of brilliant green dye using titanium based ternary metal oxide photocatalyst. *Results Phys* 12:1850–1858. <https://doi.org/10.1016/j.rinp.2019.01.065>
- Brombilla VL, Lazarotto JS, Silvestri S, Anschau KF, Dotto GL, Foletto EL (2022) Biochar derived from yerba-mate (*Ilex paraguariensis*) as an alternative TiO<sub>2</sub> support for enhancement of photocatalytic activity toward Rhodamine-B degradation in water. *Chem Eng Commun* 209:334–347. <https://doi.org/10.1080/00986445.2021.1966423>
- Chawla A, Sudhaik A, Raizada P, Ahamad T, Le Q, Nguyen VH, Singh P (2023) Bi-rich Bi<sub>2</sub>O<sub>3</sub>-based photocatalysts for energy conversion and environmental remediation: a review. *Coord Chem Rev* 491:215246. <https://doi.org/10.1016/j.ccr.2023.215246>
- Dutta V, Sonu S, Raizada P, Thakur VK, Ahamad T, Thakur S, Singh P (2022) Prism-like integrated Bi<sub>2</sub>WO<sub>6</sub> with Ag-CuBi<sub>2</sub>O<sub>4</sub> on carbon nanotubes (CNTs) as an efficient and robust S-scheme interfacial charge transfer photocatalyst for the removal of organic pollutants from wastewater. *Environ Sci Pollut Res*. <https://doi.org/10.1007/s11356-022-20743-8>
- Foo CY, Lim HN, Mahdi MAB, Chong KF, Huang NM (2016) High-performance supercapacitor based on three-dimensional hierarchical rGO/nickel cobaltite nanostructures as electrode materials. *J Phys Chem C* 120(38):21202–21210. <https://doi.org/10.1021/acs.jpcc.6b05930>
- Georgin J, Franco DSP, Netto MS et al (2021a) Transforming shrub waste into a high-efficiency adsorbent: application of *Physalis peruviana* chalice treated with strong acid to remove the 2,4-dichlorophenoxyacetic acid herbicide. *J Environ Chem* 9:104574. <https://doi.org/10.1016/j.jece.2020.104574>
- Georgin J, Salomón Y, Franco DSP et al (2021b) Successful adsorption of bright blue and methylene blue on modified pods of *Caesalpinia echinata* in discontinuous system. *Environ Sci Pollut Res* 28:8407–8420. <https://doi.org/10.1007/s11356-020-11210-3>
- Gottimukkala KSV, Harika RP, Zamare D (2017) Green synthesis of iron nanoparticles using green tea leaves extract. *J Nanomed Biotechnol Discov* 7:151. <https://doi.org/10.4172/2155-983X.1000151>
- Hassanien R, Husein DZ, Khamis M (2019) Novel green route to synthesize cadmium oxide@graphenenanocomposite: optical properties and antimicrobial activity. *Mater Res Exp* 6(8):085094. <https://doi.org/10.1088/2053-1591/ab23ac>
- Husein DZ, Hassanien R, Khamis M (2021) Cadmium oxide nanoparticles/graphene composite: synthesis, theoretical insights into reactivity and adsorption study. *RSC Adv* 11(43):27027–27041. <https://doi.org/10.1039/D1RA04754J>
- Iro ZS, Subramani C, Dash SS (2016) A brief review on electrode materials for supercapacitor. *Int J Electrochem Sci* 11(12):10628–10643. <https://doi.org/10.20964/2016.12.50>
- Ishaq S, Moussa M, Kanwal F, Ehsan M, Saleem M, Van TN, Losic D (2019) Facile synthesis of ternary graphene nanocomposites with doped metal oxide and conductive polymers as electrode materials for high performance supercapacitors. *Sci Rep* 9(1):5974. <https://doi.org/10.1038/s41598-019-41939-y>
- Jarvin M, Kumar SA, Rosaline DR, Foletto EL et al (2022) Remarkable sunlight-driven photocatalytic performance of Ag-doped ZnO nanoparticles prepared by green synthesis for degradation of emerging pollutant in water. *Environ Sci Pollut Res* 29:57330–57344. <https://doi.org/10.1007/s11356-022-19796-6>
- Jarvin M, Kumar SA, Vinodhkumar G, Manikandan E, Inbanathan SSR (2021) Enhanced photocatalytic performance of Hausmannite Mn<sub>3</sub>O<sub>4</sub>-rGO nanocomposite in degrading methylene blue. *Mater Lett* 305:130750. <https://doi.org/10.1016/j.matlet.2021.130750>
- Jarvin M, Rosaline DR, Gopalakrishnan T et al (2023) Remarkable photocatalytic performances towards pollutant degradation under sunlight and enhanced electrochemical properties of TiO<sub>2</sub>/polymer



- nanohybrids. *Environ Sci Pollut Res* 30:62832–62846. <https://doi.org/10.1007/s11356-023-26486-4>
- Jiang H, Ma J, Li C (2012) Mesoporous carbon incorporated metal oxide nanomaterials as supercapacitor electrodes. *Adv Mater* 8:4197–4202. <https://doi.org/10.1002/adma.201104942>
- Jorfi S, Barzegar G, Ahmadi M, Soltani RDC, Takdastan A, Saeedi R, Abtahi M (2016) Enhanced coagulation-photocatalytic treatment of Acid red 73 dye and real textile wastewater using UVA/synthesized MgO nanoparticles. *J Environ Manag* 177:111–118. <https://doi.org/10.1016/j.jenvman.2016.04.005>
- Karthik K, Dhanuskodi S, Gobinath C, Prabukumar S, Sivaramakrishnan S (2017) Andrographispaniculata extract mediated green synthesis of CdO nanoparticles and its electrochemical and antibacterial studies. *J Mater Sci Mater Electron* 28:7991–8001. <https://doi.org/10.1007/s10854-017-6503-8>
- Kartick B, Srivastava SK (2011) Simple facile route for the preparation of graphite oxide and graphene. *J Nanosci Nanotechnol* 11(10):8586–8592. <https://doi.org/10.1166/jnn.2011.4959>
- Kaviyarasu K, Manikandan E, Paulraj P, Mohamed SB, Kennedy J (2014) One dimensional well-aligned CdO nanocrystal by solvothermal method. *J Alloys Compd* 593:67–70. <https://doi.org/10.1016/j.jallcom.2014.01.071>
- Khan SA, Shahid S, Shahid B, Fatima U, Abbasi SA (2020) Green synthesis of MnO nanoparticles using abutilon indicum leaf extract for biological, photocatalytic, and adsorption activities. *Biomolecules* 10(5):785. <https://doi.org/10.3390/biom10050785>
- Kim CH, Kim BH (2015) Zinc oxide/activated carbon nanofiber composites for high-performance supercapacitor electrodes. *J Power Sources* 274:512–520. <https://doi.org/10.1016/j.jpowsour.2014.10.126>
- Krasil'nikov VN, Baklanova IV, Zhukov VP, Gyrdasova OI, Dyachkova TV, Tyutyunnik AP (2021) Thermally stimulated infrared shift of cadmium oxide optical absorption band edge. *Mater Sci Semicond Process* 124:105605. <https://doi.org/10.1016/j.mssp.2020.105605>
- Kumar S, Ahmed B, Ojha AK, Das J, Kumar A (2017) Facile synthesis of CdO nanorods and exploiting its properties towards supercapacitor electrode materials and low power UV irradiation driven photocatalysis against methylene blue dye. *Mater Res Bull* 90:224–231. <https://doi.org/10.1016/j.materresbull.2017.02.044>
- Kumar S, Ojha AK, Walkenfort B (2016) Cadmium oxide nanoparticles grown in situ on reduced graphene oxide for enhanced photocatalytic degradation of methylene blue dye under ultraviolet irradiation. *J Photochem Photobiol B Biol* 159:111–119. <https://doi.org/10.1016/j.jphotobiol.2016.03.025>
- Kumar SA, Jarvin M, Sharma S, Umar A, Inbanathan SSR, Lalla NP (2021) Facile and green synthesis of MgO nanoparticles for the degradation of victoria blue dye under UV irradiation and their antibacterial activity. *ES Food Agrofor* 5:14–19. <https://doi.org/10.30919/esfaf519>
- Kumar Y, Sudhaik A, Sharma K, Raizada P, Khan AAP, Nguyen VH, Asiri AM (2023) Construction of magnetically separable novel arrow down dual S-scheme ZnIn<sub>2</sub>S<sub>4</sub>/BiOCl/FeVO<sub>4</sub> heterojunction for improved photocatalytic activity. *J Photochem Photobiol A Chem* 435:114326. <https://doi.org/10.1016/j.jphotochem.2022.114326>
- Lazarotto JS, Brombilla VL, Silvestri S et al (2020) Conversion of spent coffee grounds to biochar as promising TiO<sub>2</sub> support for effective degradation of diclofenac in water. *Appl Organomet Chem* 34(12):e6001. <https://doi.org/10.1002/aoc.6001>
- Li X, Yu J, Wageh S, Al-Ghamdi AA, Xie J (2016) Graphene in photocatalysis: a review. *Small* 12(48):6640–6696. <https://doi.org/10.1002/smll.201600382>
- Ma W, Chen S, Yang S, Chen W, Weng W, Cheng Y, Zhu M (2017) Flexible all-solid-state asymmetric supercapacitor based on transition metal oxide nanorods/reduced graphene oxide hybrid fibers with high energy density. *Carbon* 113:151–158. <https://doi.org/10.1016/j.carbon.2016.11.051>
- Mageshwari K, Mali SS, Sathyamoorthy R, Patil PS (2013) Template-free synthesis of MgO nanoparticles for effective photocatalytic applications. *Powder Technol* 249:456–462. <https://doi.org/10.1016/j.powtec.2013.09.016>
- Mandal RK, Ghosh S, Majumder TP (2023) Comparative study between degradation of dyes (MB, MO) in monotonous and binary solution employing synthesized bimetallic (Fe–CdO) NPs having antioxidant property. *Results Chem* 5:100788. <https://doi.org/10.1016/j.rechem.2023.100788>
- Mariamamm RN, Susila VM, Ramachandran K (2011) On the Debye-Waller factor and Debye temperature of CdO nanoparticles. *Cryst Res Technol* 46(9):979–985. <https://doi.org/10.1002/crat.201100138>
- McCusker LB, Von Dreele RB, Cox DE, Louër D, Scardi P (1999) Rietveld refinement guidelines. *J Appl Crystallogr* 32(1):36–50. <https://doi.org/10.1107/S0021889806045493>
- Moussavi G, Mahmoudi M (2009) Removal of azo and anthraquinone reactive dyes from industrial wastewaters using MgO nanoparticles. *J Hazard Mater* 168(2–3):806–812. <https://doi.org/10.1016/j.jhazmat.2009.02.097>
- Munawar T, Rehman MN, Nadeem MS, Mukhtar F, Manzoor S, Ashiq MN, Iqbal F (2021) Facile synthesis of Cr-Co co-doped CdO nanowires for photocatalytic, antimicrobial, and supercapacitor applications. *J Alloys Compd* 885:160885. <https://doi.org/10.1016/j.jallcom.2021.160885>
- Nagabhushana H, Basavaraj RB, Prasad BD, Sharma SC, Premkumar HB, Vijayakumar GR (2016) Facile EGCG assisted green synthesis of raspberry shaped CdO nanoparticles. *J Alloys Compd* 669:232–239. <https://doi.org/10.1016/j.jallcom.2016.01.201>
- Naseem T, Farrukh MA (2015) Antibacterial activity of green synthesis of iron nanoparticles using Lawsonianermis and Gardenia jasminoides leaves extract. *J Chem*:912342. <https://doi.org/10.1155/2015/912342>
- Nasrullah M, Gul FZ, Hanif S, Mannan A, Naz S, Ali JS, Zia M (2020) Green and chemical syntheses of CdO NPs: a comparative study for yield attributes, biological characteristics, and toxicity concerns. *ACS Omega* 5(11):5739–5747. <https://doi.org/10.1021/acsomega.9b03769>
- Nuernberg G, Fajardo HV, Foletto EL et al (2011) Methane conversion to hydrogen and nanotubes on Pt/Ni catalysts supported over spinel MgAl<sub>2</sub>O<sub>4</sub>. *Catal Today* 176:36–40. <https://doi.org/10.1016/j.cattod.2010.10.053>
- Packiaraj R, Devendran P, Venkatesh KS, Bahadur SA, Manikandan A, Nallamuthu N (2019) Electrochemical investigations of magnetic Co<sub>3</sub>O<sub>4</sub> nanoparticles as an active electrode for supercapacitor applications. *J Supercond Nov Magn* 32:2427–2436. <https://doi.org/10.1007/s10948-018-4963-6>
- Paredes P, Rauwel E, Wragg DS et al (2023) Sunlight-driven photocatalytic degradation of methylene blue with facile one-step synthesized Cu-Cu<sub>2</sub>O-Cu<sub>3</sub>N nanoparticle mixtures. *Nanomaterials* 13(8):1311. <https://doi.org/10.3390/nano13081311>
- Poudel MB, Yu C, Kim HJ (2020) Synthesis of conducting bifunctional polyaniline@Mn-TiO<sub>2</sub> nanocomposites for supercapacitor electrode and visible light driven photocatalysis. *Catalysts* 10(5):546. <https://doi.org/10.3390/catal10050546>
- Pugazhendhi A, Prabhu R, Muruganatham K, Shanmuganathan R, Natarajan S (2019) Anticancer, antimicrobial and photocatalytic activities of green synthesized magnesium oxide nanoparticles (MgONPs) using aqueous extract of Sargassumwightii. *J Photochem Photobiol B Biol* 90:86–97. <https://doi.org/10.1016/j.jphotobiol.2018.11.014>
- Rane YN, Shende DA, Raghuvanshi MG, Koli RR, Gosavi SR, Deshpande NG (2019) Visible-light assisted CdO nanowires photocatalyst for toxic dye degradation studies. *Optik* 179:535–544. <https://doi.org/10.1016/j.ijleo.2018.10.215>
- Rosaline DR, Suganthi A, Vinodhkumar G et al (2022) Enhanced sunlight-driven photocatalytic activity of SnO<sub>2</sub>-Sb<sub>2</sub>O<sub>3</sub> composite

- towards emerging contaminant degradation in water. *J Alloys Compd* 897:162935. <https://doi.org/10.1016/j.jallcom.2021.162935>
- Sadhukhan S, Ghosh TK, Roy I, Rana D, Bhattacharyya A, Saha R, Chattopadhyay D (2019) Green synthesis of cadmium oxide decorated reduced graphene oxide nanocomposites and its electrical and antibacterial properties. *Mater Sci Eng C* 99:696–709. <https://doi.org/10.1016/j.msec.2019.01.128>
- Salomón YO, Georjín J, Franco DSP et al (2021) Application of seed residues from *Anadenanthera macrocarpa* and *Cedrela fissilis* as alternative adsorbents for remarkable removal of methylene blue dye in aqueous solutions. *Environ Sci Pollut Res* 28:2342–2354. <https://doi.org/10.1007/s11356-020-10635-0>
- Santos SBF, Hollanda LR, Vieira Y et al (2023) Enhanced UV-light driven photocatalytic performance of magnetic  $\text{CoFe}_2\text{O}_4/\text{TiO}_2$  nanohybrid for environmental applications. *Environ Sci Pollut Res* 30:75078–75088. <https://doi.org/10.1007/s11356-023-27762-z>
- Shad NA, Sajid MM, Haq AU, Amin N, Imran Z, Anwar H, Javed Y (2019) Photocatalytic investigation of cadmium oxide nanosheets prepared by hydrothermal method. *Arab J Sci Eng* 44:6669–6675. <https://doi.org/10.1007/s13369-019-03897-5>
- Silvestri S, Oliveira JF, Foletto EL (2019b) Degradation of methylene blue using  $\text{Zn}_2\text{SnO}_4$  catalysts prepared with pore-forming agents. *Mater Res Bull* 117:56–62. <https://doi.org/10.1016/j.materresbull.2019.04.033>
- Silvestri S, Stefanello N, Salla JS et al (2019a) Photocatalytic properties of  $\text{Zn}_2\text{SnO}_4$  powders prepared by different modified hydrothermal routes. *Res Chem Intermed* 45:4299–4313. <https://doi.org/10.1007/s11164-019-03832-1>
- Silvestri S, Stefanello N, Sulkovski AA, Foletto EL (2020) Preparation of  $\text{TiO}_2$  supported on MDF biochar for simultaneous removal of methylene blue by adsorption and photocatalysis. *J Chem Technol Biotechnol* 95:2723–2729. <https://doi.org/10.1002/jctb.6279>
- Simon R, Chakraborty S, Darshini KS, Mary NL (2020) Electrolyte dependent performance of graphene–mixed metal oxide composites for enhanced supercapacitor applications. *SN Appl Sci* 2:1–11. <https://doi.org/10.1007/s42452-020-03708-9>
- Singh J, Kumar V, Kim KH, Rawat M (2019) Biogenic synthesis of copper oxide nanoparticles using plant extract and its prodigious potential for photocatalytic degradation of dyes. *Environ Res* 177:108569. <https://doi.org/10.1016/j.envres.2019.108569>
- Sudhaik A, Raizada P, Rangabhashiyam S, Singh A, Nguyen VH, Van Le Q, Singh P (2022) Copper sulfides based photocatalysts for degradation of environmental pollution hazards: a review on the recent catalyst design concepts and future perspectives. *Surf Interf*:102182. <https://doi.org/10.1016/j.surfin.2022.102182>
- Sutradhar P, Saha M, Maiti D (2014) Microwave synthesis of copper oxide nanoparticles using tea leaf and coffee powder extracts and its antibacterial activity. *J Nanostructure Chem* 4:1–6. <https://doi.org/10.1007/s40097-014-0086-1>
- Tadjarodi A, Akhavan O, Bijanzad K (2015) Photocatalytic activity of CuO nanoparticles incorporated in mesoporous structure prepared from bis(2-aminonicotinato) copper (II) microflakes. *Trans Nonferrous Metals Soc China* 25(11):3634–3642. [https://doi.org/10.1016/S1003-6326\(15\)64004-3](https://doi.org/10.1016/S1003-6326(15)64004-3)
- Taurati R, Khaddor M, Laghzal A, El Kasmi A (2020) Facile one-step synthesis of highly efficient single oxide nanoparticles for photocatalytic application. *Sci African* 8:e00305. <https://doi.org/10.1016/j.sciaf.2020.e00305>
- Thema FT, Beukes P, Gurib-Fakim A, Maaza M (2015) Green synthesis of Monteponite CdO nanoparticles by *Agathosmabetulina* natural extract. *J Alloys Compd* 646:1043–1048. <https://doi.org/10.1016/j.jallcom.2015.05.279>
- Umar A, Kumar SA, Inbanathan SSR, Modarres M, Kumar R, Algadi H, Baskoutas S (2022a) Enhanced sunlight-driven photocatalytic, supercapacitor and antibacterial applications based on graphene oxide and magnetite-graphene oxide nanocomposites. *Ceram Int* 48(19):29349–29358. <https://doi.org/10.1016/j.ceramint.2022.05.371>
- Umar A, Kumar SA, Rosaline DR et al (2022b) Poly(1-Naphthylamine) nanoparticles as potential scaffold for supercapacitor and photocatalytic applications. *Micromachines* 13(9):1528. <https://doi.org/10.3390/mi13091528>
- Veerakumar P, Sangili A, Manavalan S, Thanasekaran P, Lin KC (2020) Research progress on porous carbon supported metal/metal oxide nanomaterials for supercapacitor electrode applications. *Ind Eng Chem Res* 59(14):6347–6374. <https://doi.org/10.1021/acs.iecr.9b06010>
- Vieira Y, Rossatto DL, Leichtweis J et al (2022) Iron-enriched coal and volcanic rock waste powder composite with enhanced microwave absorption capacity for the degradation of 2,4-D and atrazine pesticides in single and binary systems. *Adv Powder Technol* 33:103671. <https://doi.org/10.1016/j.apt.2022.103671>
- Wadekar PH, Khose RV, Pethsangave DA, Some S (2020) Waste-derived heteroatom-doped activated carbon/manganese dioxide trio-composite for supercapacitor applications. *Energy Technol* 8(6):1901402. <https://doi.org/10.1002/ente.201901402>
- Wei D, Liu Y (2010) Controllable synthesis of graphene and its applications. *Adv Mater* 22(30):3225–3241. <https://doi.org/10.1002/adma.200904144>
- Xiang Q, Yu J (2013) Graphene-based photocatalysts for hydrogen generation. *J Phys Chem Lett* 4(5):753–759. <https://doi.org/10.1021/jz302048d>
- Yuan A, Zhang Q (2006) A novel hybrid manganese dioxide/activated carbon supercapacitor using lithium hydroxide electrolyte. *Electrochem Commun* 8(7):1173–1178. <https://doi.org/10.1016/j.elecom.2006.05.018>
- Zhi M, Xiang C, Li J, Li M, Wu N (2013) Nanostructured carbon–metal oxide composite electrodes for supercapacitors: a review. *Nanoscale* 5(1):72–88. <https://doi.org/10.1039/C2NR32040A>
- Zhou X, Zhang X, Wang Y, Wu Z (2021) 2D graphene- $\text{TiO}_2$  composite and its photocatalytic application in water pollutants. *Front Energy Res* 8:612512. <https://doi.org/10.3389/fenrg.2020.612512>

**Publisher's Note** Springer Nature remains neutral with regard to jurisdictional claims in published maps and institutional affiliations.

Springer Nature or its licensor (e.g. a society or other partner) holds exclusive rights to this article under a publishing agreement with the author(s) or other rightsholder(s); author self-archiving of the accepted manuscript version of this article is solely governed by the terms of such publishing agreement and applicable law.